Heliyon 10 (2024) e35255

Contents lists available at ScienceDirect

Heliyon

journal homepage: www.cell.com/heliyon

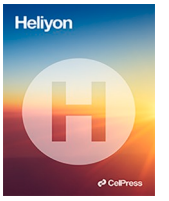

Research article

Cucumis melo compounds: A new avenue for ALR-2 inhibition in diabetes mellitus

Khalid Alshaghdali [a,1], Munazzah Tasleem [b,1], Raja Rezgui [a], Talal Alharazi [a,i], Tolgahan Acar [c], Raed Fahad Aljerwan [d], Ahmed Altayyar [d], Samra Siddiqui [e], Mohd Saeed [f,j,*], Dharmendra Kumar Yadav [h,**], Amir Saeed [a,g]

[a] *Department of Clinical Laboratory Sciences, College of Applied Medical Sciences, University of Hail, Hail, Saudi Arabia*
[b] *Department of Biochemistry, Jamia Hamdard, Delhi, India*
[c] *Department of Physical Therapy, College of Applied Medical Sciences, University of Hail, Hail, Saudi Arabia*
[d] *Regional Laboratory, Ministry of Health, Hail, Saudi Arabia*
[e] *Department of Health Service Management, College of Public Health and Health Informatics, University of Hail, Hail, Saudi Arabia*
[f] *Department of Biology, College of Sciences, University of Hail, Hail, Saudi Arabia*
[g] *Department of Medical Microbiology, Faculty of Medical Laboratory Sciences, University of Medical Science & Technology, Khartoum, Sudan*
[h] *College of Pharmacy, Gachon University of Medicine and Science, Hambakmoeiro, Yeonsugu, Incheon City, 21924, South Korea*
[i] *Department of Medical Microbiology and Immunology, Faculty of Medicine and Health Sciences, Taiz University, Taiz, Yemen*
[j] *Centre for Global Health Research Saveetha Medical College Chennai - 602105, Tamil Nadu India*

ARTICLE INFO

Keywords:
Cucumis melo
Aldose reductase (ALR2)
ADMET
Docking
MD simulation

ABSTRACT

Diabetes mellitus (DM) is a prominent contributor to morbidity and mortality in developed nations, primarily attributable to vascular complications such as atherothrombosis occurring in the coronary arteries. Aldose reductase (ALR2), the main enzyme in the polyol pathway, catalyzes the conversion of glucose to sorbitol, leading to a significant buildup of reactive oxygen species in different tissues. It is therefore a prime candidate for therapeutic targeting, and extensive study is currently underway to discover novel natural compounds that can inhibit it. *Cucumis melo (C. melo)* has a long history as a lipid-lowering ethanopharmaceutical plant. In this study, compounds derived from *C. melo* were computationally evaluated as possible lead candidates. Various computational filtering methods were employed to assess the drug-like properties and ADMET (absorption, distribution, metabolism, excretion, and toxicity) profiles of the compounds. The compounds were subsequently addressed to analysis of their interactions, molecular docking, and molecular dynamics simulation studies. When compared to the conventional therapeutic compounds, three compounds exhibited enhanced binding affinity and intra-molecular residue interactions, resulting in increased stability and specificity. Consequently, four potent inhibitors, namely PubChem CIDs 119205, 65373, 6184, and 332427, have been identified. These inhibitors exhibit promising potential as pharmacological targets for the advancement of novel ALR-2 inhibitors.

* Corresponding author. Department of Biology, College of Sciences, University of Hail, Hail, Saudi Arabia.
** Corresponding author.
E-mail address: mo.saeed@uoh.edu.sa (M. Saeed).
[1] Equal Contribution.

https://doi.org/10.1016/j.heliyon.2024.e35255
Received 12 November 2023; Received in revised form 24 July 2024; Accepted 25 July 2024
Available online 27 July 2024

1. Introduction

Diabetes mellitus (DM) is the most widespread endocrine disease, a diverse set of metabolic abnormalities of proteins, lipids, and carbohydrates [1]. Despite a variety of therapies, diabetes prevalence has considerably increased globally [2]. DM and its associated consequences are recognized as significant contributors to global mortality and morbidity [3], (affecting about 25 % of the population) [4]. It has been observed that type 2 Diabetes mellitus (T2DM) or non-insulin-dependent diabetes affects about 90 % of the population [5]. Around 463 million cases of T2DM were reported in 2019, and by 2040, that number is expected to rise to 642 million [6,7].

Diabetic peripheral neuropathy (DPN) is a commonly observed complication of diabetes mellitus (DM). The upregulation of the polyol and hexosamine pathways leads to various consequences, including elevated levels of non-enzymatic glycation products, increased activity of protein kinase C, and the development of complications associated with diabetes [8]. Pathological characteristics of diabetic peripheral neuropathy (DPN) include axonal atrophy, demyelination, and the delayed regeneration of peripheral sensory nerve fibers. A modest metabolic flow through the polyol pathway characterizes normoglycemia. The reason for this is that glucose-6-phosphate has a lower binding strength than glucose for the enzyme aldose reductase (ALR2, AKR1B1), which is responsible for catalyzing the initial stage of the process [9]. This alters when a person experiences hyperglycemia because high blood sugar gives ALR2 considerable amounts of substrate. The polyol pathway involves the conversion of glucose into sorbitol, which is subsequently metabolized into fructose through the action of the enzyme sorbitol dehydrogenase. The heightened synthesis of sorbitol leads to a depletion of cellular NADPH, rendering cells more susceptible to harm caused by reactive oxygen species [10], consequently inducing oxidative and osmotic stress. The potential outcomes of diabetes encompass various complications such as neuropathy, nephropathy, retinopathy, and the development of atherosclerotic plaques. Additionally, the augmented synthesis of fructose contributes to the generation of advanced glycation end products (AGEs) [11,12].

ALR-2, an enzyme that serves as a rate-limiting enzyme in the polyol pathway, has been the subject of extensive research as a pharmaceutical target for addressing complications associated with diabetes [13]. The glutathione conjugates and other aldehydes produced from lipid peroxidation are reduced by ALR2. Inhibition of ALR2 has been demonstrated to block inflammatory signals brought on by endotoxins, cytokines, autoimmune responses, hyperglycemia, and allergens in various types of cells and animal models [14]. An excessive activity of the ALR-2 enzyme within the polyol pathway has been linked to an alteration in the ratios of NADPH/NADP+ and NADH/NAD+, leading to the intensification of oxidative stress through the reduction of levels of reduced glutathione (GSH) [15]. Oxidative stress is distinguished by an augmented generation of reactive oxygen species [10] and compromised antioxidant defenses due to an imbalance between oxidative factors and antioxidant capacities [16].

Diverse ALR2 inhibitors have been investigated as possible treatment options for diabetes. Nevertheless, toxicity associated with the nonselective inhibition of ALR2 remains the primary concern. These compounds exhibit nonselective interaction with ALR1 and possess a structural similarity of 65 % with ALR2, a protein that plays a role in the metabolism of harmful lipid peroxidation byproducts like methylglyoxal and 3-oxyglucosazone. This indicates that despite the progress made in the development of numerous potent ALR2 inhibitors obtained from both synthetic and natural origins, only a restricted selection of compounds have advanced to the clinical trial phase. Currently, epalrestat stands as the sole ALR2 inhibitor that has received approval for the treatment of diabetic complications in China, India, and Japan [14].

The available medicinal products are primarily used for disease maintenance. Moreover, prolonged medication results in severe toxicity. Therefore, it is imperative to exploit plant materials and natural resources for diabetes treatment. Plants and plant-derived products possess a diverse array of bioactive secondary metabolites and exhibit multiple modes of action, thereby potentially conferring a comparative advantage. Additionally, they can be used as sources of lead compounds that could be transformed [17]. Natural compounds have been observed to engage with a wide range of biological targets, and several of these compounds have acquired significant importance as therapeutic agents [10]. Melon, or *C. melo* L., is a kind of tropical plant that is a member of the *Cucurbitaceae* family. As an ethno-pharmacological agent, it has a long history on the Indian subcontinent. As an annual plant, it thrives in a wide range of climates, including the Mediterranean, desert, subtropics, temperate, and tropical [18]. The fruit and seed have long been utilized in traditional Chinese and Indian medicine for the treatment of several ailments, including fever, eye infections, bronchitis, ulcers, and bronchial infections [19]. *C. melo* contains glycolipids, carbohydrates multiflorenol, terpenoids, flavonoids, β-carotenes, and apocaretonoids as its primary active phytoconstituents [20]. It contains antioxidant, anti-inflammatory, antibacterial, anti-hypothyroidism, and antiangiogenic properties. It has been reported to lower blood glucose level [21]. The current study was conducted to assess the potential anti-diabetic and anti-hyperlipidemic effects of compounds from *C. melo* exhibiting robust pharmacological characteristics [22]. Therefore, *in silico* approach is applied to identify and evaluate the efficacy and pharmacological properties of the potential compounds from *C. melo* to inhibit ALR2 to treat diabetic peripheral neuropathy (DPN).

2. Materials and methods

2.1. Compound retrieval

Phytochemicals from *C. melo*, retrieved from Indian Medicinal Plants, Phytochemistry and Therapeutics 2.0 (IMPPAT 2.0) (accessed on 06 January 2022) and PubChem (accessed on 12 February 2022) [23] were used in this study. (IMPPAT 2.0) the database is manually compiled and contains information retrieved from published articles, supplementary sources, and over a hundred books on traditional Indian medicine. It is freely accessible online (https://cb.imsc.res.in/imppat/) [24]. PubChem, an extensive chemical database, is managed by the National Center for Biotechnology Information (NCBI), and provides data related to the properties and biological activities of chemical compounds.

2.2. Retrieval and preparation of ALR-2 structure

The Research Collaboratory for Structural Bioinformatics (RSCB) protein data bank (http://www.rcsb.org/) was accessed (accessed on January 06, 2022) to obtain the protein ALR2 (PDB ID: 4JIR_A) [25]. The structure solved by X-ray crystallography at 2.0 Å consists of 316 residues. The binding pocket of the ALR2 was cleared of water molecules, co-crystal ligands, and inhibitors, and a sphere with a radius of 8.0 Å and coordinates of X = −5.716000, Y = 8.025769, and Z = 17.346538 was created around it. The receptor protein was cleared of water molecules and co-crystal ligands before commencing the docking process. The "Prepare protein" technique from Discovery Studio (DS) [Dassault Systems, BIOVIA Corp., San Diego, CA, USA, v 20.1.0. 20298], was used to add hydrogen, replace any missing atoms, and attach a CHARMm forcefield to the protein.

2.3. Pharmacokinetic analysis

For *in silico* drug-likeness and absorption, distribution, metabolism, excretion, toxicity (ADMET) calculations, the TOPKAT module, ADMET Descriptors, and the Filter by Lipinski and Veber Rules Module from Discovery Studio [26] [Dassault Systems, BIOVIA Corp., San Diego, CA, USA, version 21.1] were utilized to select the drug-like *C. melo* compounds. The n-octanol/water partition coefficient logarithmic (LogP), the molecular polar surface area, the number of hydrogen bond acceptors (HBA), the number of hydrogen bond donors (HBs) [27], and the number of rotatable bonds (RotB) were all calculated under Lipinski's rule of five and the Veber rule [13, 28]. These ADME and TOPKAT modules are employed to quantify the compound's characteristics such as water solubility, blood-brain barrier (BBB) permeability, hepatotoxicity, human intestinal absorption, plasma protein binding (PPB) levels, rodent carcinogenicity, and Bacterial Reverse Mutation Assay (AMES) mutagenicity [29,30].

2.4. Virtual screening of C. melo compounds and molecular docking with ALR2

One crucial first step in finding possible drug candidates that interact well with the receptor protein is the virtual screening of the compounds. This procedure takes advantage of the atomic-level interactions that molecules have with targets that are proteins. Using the CDocker module from Discovery Studio [Dassault Systems, BIOVIA Corp., San Diego, CA, USA, v 21.1], all *C. melo* compounds were virtually screened in this study to find those with promising interactions. For further examination, the best-docked position with the highest CDocker score was determined.

2.5. Scoring the docked compounds

The "Score Ligand Poses" module in the DS software was utilized to re-evaluate the highest docking pose for each molecular structure. For the estimation of ligand binding in active receptor sites, the CDOCKER Scores (CDOCK) and Ludi Energy Estimate 3 (Ludi 3) were utilized. Better binding of the compounds was denoted by higher scores, represented as positive values [31]. LUDI scoring system assigns small molecules in the binding cavity to create close intra-molecular interactions with active site residues. It can add fragments to existing ligands and create interaction sites [32]. The ligand poses were analysed using the DS module "Analyze Ligand Poses". In addition, the "Calculate Binding Energies" module of DS was used to calculate the binding energy of the docked positions. Ligand efficiency (LE) is an important parameter when choosing leads. Since the principle of drug development is incremental, this is consistent with the assumption that variations in chemical behavior among structurally similar molecules are simpler to comprehend and predict than absolute predictions to be made based on molecular structure [33]. A drug's activity is determined by its concentration, whereas the sensitivity of a reaction to its driving force is determined by its affinity. Thus, certain objectives can be specified in drug design, including maximum affinity toward the therapeutic target(s) and minimum affinity toward anti-targets [34].

2.6. Molecular dynamics simulation

The 01_control and 02_docked complexes were subjected to MD simulation using Gromacs version 2020.4. Both protein-ligand systems were solvated with TIP3P water molecules in a truncated octahedral box. The minimum distance between protein systems and the edges of the simulation box was set to 10 Å to efficiently meet the criteria for minimum image convention during MD simulation. Both protein systems were electronically neutralized by adding 29 K^+ and 26 Cl^- ions for 01_control and 28 K^+ and 26 Cl^- ions for 02_docked complexes in the environment. The protonation states were evaluated at 7.4 pH using CHARMM-GUI for His, Lys, Arg, Asp, and Glu residues and implemented after visual inspection. The systems for 01_control and 02_docked complexes contained 32929, and 32910 atoms in total, respectively. The Chemistry at HARvard Macromolecular Mechanics-Graphical User Interface (CHARMM-GUI) webserver was used to generate all input files [35,36].

All systems were minimized for 5000 steps using the Steepest Descent technique, and convergence was achieved under the force limit of 1000 (kJ/mol/nm) to exclude any steric clashes. Later, both minimized systems were separately equilibrated at NVT (Canonical ensemble: where moles, N; volume, V; and temperature, T were conserved) and NPT (Isothermal-Isobaric ensemble: where moles, N; pressure, P; and temperature, T were conserved) ensembles for 100 ps (50,000 steps) and 1000 ps (1,000,000 steps), respectively, using time steps 0.2 and 0.1 fs, at 310.15 K to ensure a fully converged system for the production run [37].

The simulation runs for both systems were conducted at a constant temperature of 310.15 K and a pressure of 1 atm, or 1 bar (using an NPT ensemble), utilizing weak coupling velocity re-scaling (modified Berendsen thermostat), and Parrinello-Rahman algorithms, respectively. The relaxation times were set at τ T = 0.1 ps and τ P = 2.0 ps. Using the LINear Constraint Solver (LINCS) algorithm, all

bond lengths involving hydrogen atoms were maintained stiffly at optimal bond lengths, with a time step of 2 fs. The non-bonded interactions were calculated using the Verlet algorithm. Interactions within a short-range cutoff of 12 Å were calculated in each time step. The electrostatic interactions and forces in a homogeneous medium beyond the short-range cutoff were calculated using the Particle Mesh Ewald (PME) method. The Periodic Boundary Conditions (PBC) were applied in all x, y, and z directions. For each of the three complexes, the production was run for 100 ns. The trajectory and energy data were recorded at every 20 ps [5]. The first 20 ns of the trajectories were excluded and the remaining 80 ns were utilized for MMGBSA. GROMACS simulation package (GROMACS 2020.4) [38], was used to perform molecular dynamics simulations using CHARMM36m forcefield [39]. GRaphing, Advanced Computation, and Exploration of data (Grace) were used to generate all plots (https://plasma-gate.weizmann.ac.il/Grace). The Molecular Mechanics Poisson-Boltzmann Surface Area (MMGBSA) protein-ligand binding energy was calculated after every 1 ns of simulations for both systems [40].

3. Results and discussion

The pharmacokinetics [26] and pharmacodynamics (PD) phases of every pharmacological substance reveal its biological response. This study includes an *in silico* analysis of the *C. melo* compounds and ALR-2 interactions at different molecular events in the PK and PD phases. As part of the in-silico PK evaluation, the acquired hits undergo comprehensive drug-likeness and ADMET profiling, which employs several fundamental criteria and techniques of DS. Through the utilization of molecular docking, intramolecular interactions, and MD simulation experiments, the PD ascertains the potency of the hits with ALR-2.

3.1. Evaluation of drug likeness and ADMET properties of the compounds

The Lipinski rule was used to assess the drug-like qualities of twenty-eight compounds from *C. melo*. To enhance outcomes, compounds that satisfied two or more of the Lipinski rule requirements were examined for their drug-like characteristics. Under Lipinski's rule of five, which explains that a molecule cannot differ from more than two of the following parameters (molecular weight (MW) < 500 Da, partition coefficient (LogP) < 5, hydrogen-bond donors (HBD) < 5, and hydrogen-bond acceptors (HBA) < 10) to be used safely as a therapeutic agent, 22 natural compounds out of 28 virtually screened compounds qualified for the drug-likeness parameter, as shown in ADMET analysis Table 1. Drug discovery is dependent on the ADMET characteristics of a compound since these characteristics account for sixty percent of drug failures in clinical trials [41]. A compound with a suitable ADME profile can enter the bloodstream through the digestive system, where it is then absorbed, digested by metabolic enzymes, and expelled from the body without interfering with healthy biological functions [28]. The ADMET descriptors module in DS is implemented to evaluate the AlogP98, BBB, aqueous solubility, PPB, polar surface area [27], hepatotoxicity, CYP2D6 enzyme inhibition, and intestinal absorption of a drug-like compound. An equation for linear regression was implemented to determine the aqueous solubility of the compounds in water at 25 °C. The therapeutic potential and intestinal absorption of compounds are determined by their solubility and absorption levels after oral administration. For intestinal absorption, the values must be 0, where 0 indicates good absorption and 1 indicates moderate absorption; for water solubility, 3 indicates good solubility and 4 indicates optimal solubility [42]. The hydrophilicity is measured by the AlogP98 value, where AlogP98 > 5 indicates a high level of absorption or permeability. PSA is an additional consideration that significantly influences drug absorption. Compounds with a PSA ≤ 140 Å can be passively ingested; consequently, they have a high oral bioavailability [43]. The BBB level approximates the amount of drug that penetrates the central nervous system (CNS) after oral administration. Due to its effect on the CNS, a desirable drug could not cross the BBB. Consequently, the best

Table 1
Pharmacokinetic properties of selected *C. melo* compounds retrieved from PubChem.

PubChem CID	ALogP	PSA	Mol. Weight	H Acceptors	H Donors	Rotatable bonds
6434541	2.362	20.23	140.223	1	1	5
225688	7.349	20.23	426.717	1	1	0
225689	7.303	20.23	426.717	1	1	0
14328	1.537	35.53	180.2	3	0	3
31226	2.382	26.3	178.228	2	0	5
16219576	7.403	20.23	426.717	1	1	1
5283637	7.627	20.23	400.68	1	1	5
3080632	8.084	20.23	414.707	1	1	6
94204	7.859	20.23	440.744	1	1	5
521229	7.639	20.23	412.691	1	1	5
177	−0.183	17.07	44.0526	1	0	0
60961	−1.881	139.54	267.241	7	4	2
5362720	2.776	17.07	140.223	1	0	6
17750995	7.553	20.23	426.717	1	1	4
702	−0.01	20.23	46.0684	1	1	0
6184	1.853	17.07	100.159	1	0	4
11876210	7.498	20.23	426.717	1	1	0
23724573	7.431	20.23	398.664	1	1	5
Epalrestat	3.442		319.399	5	1	4

Abbreviations: ALogP- n-octanol-water partition coefficients; PSA- Polar Surface Area; Mol. Weight- Molecular weight; H- Hydrogen.

therapeutic molecules for administration tend to be those with BBB scores of 3 or 2 (low or medium) [44], as shown in Table 1.

Typically, drug toxicity is predicted based on the propensity of a drug compound to induce dose-dependent liver damage, which can be utilized to assess its hepatotoxicity. The metabolism of drugs is governed by CYP450 isoforms and enzymes. The inhibition of these detoxification enzymes could potentially lead to toxic effects [45]. CYP2D6 comprises only 2 % of the entire CYP concentration; however, it is responsible for the biotransformation of 20 % of pharmaceuticals metabolized in the liver. A total of five CYP isoforms (3A4, 2D6, 2C19, 2C9, and 1A2) are responsible for the oxidative metabolism of over 80 % of clinically tested drugs. In this study, only one compound PubChem CID: 521229, blocked the CYP2D6 enzyme, and three compounds viz, PubChem CID: 177, 60961, and 702 were observed to be associated with hepatotoxicity. The degree of interaction between a drug and blood protein receptors is denoted by the PPB. Efficacy might be impacted by the degree of binding exhibited by a substance. The classification of "false" and "true," respectively, was based on the PPB values of drug molecules that were "highly" and "poorly" bound, as shown in Table 2.

For the assessment of potential mutagenicity, reproductive or developmental toxicity, ecotoxicity, and mutagenicity in therapeutic candidates, the TOPKAT method is widely utilized. The findings from the ADMET and TOPKAT analyses indicate that the estimated levels of carcinogenicity exhibited by the filtered compounds fall within the anticipated range, and no indications of mutagenicity are present. However, some compounds may cause minor skin irritation, mild to severe eye irritation, and developmental or reproductive damage if used for an extended period of time or in higher concentrations. The additional toxicity screening properties of *C. melo* compounds are listed in Table 3. More than half of the filtered compounds were found to be non-mutagenic, biodegradable, mildly to moderately irritating to the skin and eyes, non-toxic, and non-carcinogenic.

3.2. Targeted compound selection and interaction analysis in C. melo derived compounds

A critical component of our drug discovery methodology involved the virtual screening of compounds derived from *C. melo,* which was performed before the initiation of molecular docking and interaction studies. This helps in identifying molecules that have the potential to interact effectively with the target protein. The targeted selection of promising candidates for additional research is made possible by this strategic approach. This first step can be thought of as a screening process that will assist us in selecting the best candidates from among the many available. With its low cost and obvious ease of use, molecular docking is becoming increasingly popular among academic groups as a method of discovering new drugs [46]. Target protein-small drug-like molecule binding was predicted using molecular docking [47]. Given the importance of protein dysfunction in various diseases, therapeutic approaches frequently involve modulating specific proteins through inhibition or activation [48]. Ten compounds from *C. melo* out of twenty-two were observed to dock in the binding pocket of ALR2. For intramolecular interaction studies, the compounds with a high -CDocker score, LUDI score, and ligand efficiency were selected. These analyses had the goal of determining the protein's binding preferences and intramolecular interactions with the newly discovered compounds in order to rule out any false positives [49]. The expected modes of ligand-protein binding at the active site are determined via molecular docking experiments.

The grid-based docking technique CDOCKER maximizes docking for a single receptor protein in the presence of multiple ligands. Random rotations and high-temperature molecular dynamics generate arbitrary ligand conformations during molecular docking. We use grid-based (GRID 1) simulated annealing to study random rotations. The random rotations are further studied employing simulated annealing on a grid-based (GRID 1) platform. To validate the docking procedure, the bound ligand epalrestat, was re-docked in the binding pocket of the receptor protein ALR2 (PDB ID: 4JIR_A). The superimposed binding pose of the epalrestat shown in Fig. S1,

Table 2
Estimated druglikeness properties of *C. melo* compounds.

Name	Solubility	Absorption	BBB	AlogP98	CYP2D6	Hepatotoxic	PPB
6434541	4	0	1	0	F	F	T
225688	0	3	4	0	F	F	T
225689	0	3	4	0	F	F	T
14328	3	0	2	0	F	F	T
31226	3	0	1	0	F	F	T
16219576	0	3	4	0	F	F	T
31226	3	0	1	0	F	F	T
5283637	1	3	4	0	F	F	T
3080632	0	3	4	0	F	F	T
94204	0	3	4	0	F	F	T
521229	1	3	4	0	T	F	T
177	5	2	4	0	F	T	F
60961	4	2	4	0	F	T	F
5362720	3	0	1	0	F	F	F
17750995	0	3	4	0	F	F	T
702	5	1	4	0	F	T	F
6184	4	0	1	0	F	F	F
11876210	0	3	4	0	F	F	T
23724573	1	3	4	0	F	F	T
Epalrestat	4	1	3	1	F	T	F

Abbreviations: ALogP- n-octanol-water partition coefficients; BBB- Blood Brain Barrier; PSA-Polar Surface Area; CYP2D6-Cytochrome P450 2D6; PPB-Plasma Protein Binding; F-False; T-True.

Table 3
Toxicity parameters evaluated for *C. melo* compounds.

Name	Rat Female NTP	Rat Male NTP	Mutagenicity	DTP	Skin Irritancy	Ocular Irritancy	Biodegradability
6434541	Non-Carcinogen	Non-Carcinogen	Non-Mutagen	Non-Toxic	Moderate	Moderate	Degradable
225688	Non-Carcinogen	Carcinogen	Non-Mutagen	Toxic	Moderate	Severe	Degradable
225689	Non-Carcinogen	Non-Carcinogen	Non-Mutagen	Toxic	Moderate	Severe	Degradable
14328	Non-Carcinogen	Carcinogen	Non-Mutagen	Toxic	Mild	Mild	Degradable
31226	Non-Carcinogen	Non-Carcinogen	Non-Mutagen	Non-Toxic	Moderate	Mild	Degradable
16219576	Non-Carcinogen	Non-Carcinogen	Non-Mutagen	Toxic	Moderate	None	Degradable
31226	Non-Carcinogen	Non-Carcinogen	Non-Mutagen	Non-Toxic	Moderate	Mild	Degradable
5283637	Non-Carcinogen	Non-Carcinogen	Non-Mutagen	Toxic	Moderate	Severe	Degradable
3080632	Non-Carcinogen	Non-Carcinogen	Non-Mutagen	Toxic	Moderate	None	Degradable
94204	Non-Carcinogen	Non-Carcinogen	Non-Mutagen	Toxic	Moderate	None	Degradable
521229	Non-Carcinogen	Non-Carcinogen	Non-Mutagen	Toxic	Moderate	Moderate	Degradable
177	Carcinogen	Carcinogen	Non-Mutagen	Toxic	Mild	Moderate	Non-Degradable
60961	Non-Carcinogen	Carcinogen	Non-Mutagen	Non-Toxic	Mild	Moderate	Degradable
5362720	Non-Carcinogen	Carcinogen	Non-Mutagen	Non-Toxic	Moderate	None	Degradable
17750995	Non-Carcinogen	Non-Carcinogen	Non-Mutagen	Toxic	Moderate	None	Degradable
702	Non-Carcinogen	Carcinogen	Non-Mutagen	Toxic	Mild	Severe	Degradable
6184	Non-Carcinogen	Non-Carcinogen	Non-Mutagen	Non-Toxic	Moderate	Mild	Degradable
11876210	Non-Carcinogen	Non-Carcinogen	Non-Mutagen	Toxic	Moderate	None	Degradable
23724573	Non-Carcinogen	Non-Carcinogen	Non-Mutagen	Toxic	Moderate	None	Degradable
65373	Non-Carcinogen	Non-Carcinogen	Non-Mutagen	Non-Toxic	Mild	Mild	Degradable
332427	Non-Carcinogen	Non-Carcinogen	Non-Mutagen	Non-Toxic	Severe	Moderate	Non-Degradable
73399	Non-Carcinogen	Non-Carcinogen	Non-Mutagen	Non-Toxic	Severe	Severe	Non-Degradable
119205	Non-Carcinogen	Non-Carcinogen	Non-Mutagen	Non-Toxic	Severe	Moderate	Degradable
Epalrestat	Non-Carcinogen	Non-Carcinogen	Non-Mutagen	Toxic	Moderate	Moderate	Degradable

demonstrate the robustness the tool CDOCKER.

It was discovered that the compounds with the PubChem CID 119205, 65373, 6184, and 332427 had a -CDOCKER energy that was comparable to that of epalrestat, however it established a greater number of hydrogen bonds and hydrophobic interactions with the binding site residues, which improved the compound's stability, affinity, and specificity [26]. Through the docking simulations, the compounds of *C. melo* were examined for their binding affinities within the ALR2 binding pocket. The results were determined based on the CDocker score, binding energy, ligand efficiency score, and LUDI score. Notably, the top-ranked compound CID: 119205, exhibited the highest CDocker score of 30.8343 and the most favorable binding energy of −145.23 kcal/mol among the tested compounds. The Ligand Efficiency Score of 81.2, indicates its potential as a high-affinity ligand. In addition, the LUDI analysis revealed significant interactions between the ligand and crucial residues in the ALR2 binding pocket. These interactions involve hydrogen bonds with Leu301, Gln183, and Lys77, as well as pi-pi stacking interactions with Phe122, Tyr209, and Tyr48. These findings indicate a high affinity between 119205 and the ALR2 binding pocket. In a similar manner, compound 65373 exhibited a significant CDocker score of 25.3692 and a binding energy of −120.23 kcal/mol. With slightly lower scores compared to 119205, 65373 showed significant interactions with residues like Leu301, Ser302, and Gln183, suggesting its potential as a promising ligand candidate. On the other hand, compounds 6184 and 332427 showed weaker binding affinities, with CDocker scores of 18.67 and 15.3902, respectively. These compounds showed relatively weaker interactions with ALR2 binding pocket residues, leading to lower binding energies and ligand efficiency scores. Epalrestat showed a remarkably high binding energy of −148.18 kcal/mol, indicating a strong binding affinity, despite having a lower CDocker score (14.17) when compared to the top-ranked *C. melo* compound 119205. On the other hand, the ligand efficiency score of epalrestat (33.56) was significantly lower compared to 119205, indicating a less efficient utilization of binding interactions within the ALR2 binding pocket. The interaction profile of epalrestat revealed hydrogen bond interactions with Tyr48, His110, and Trp111, suggesting specific molecular interactions within the ALR2 binding pocket. Additionally, electrostatic interactions with His110, pi-pi stacking interactions with Trp20, and pi-alkyl interactions with Phe122 and Cys298 were observed. These interactions collectively contribute to the stability of epalrestat within the binding pocket of ALR2. In comparison, the top-ranked *C. melo* compound, 119205, exhibited promising binding characteristics comparable to or even surpassing Epalrestat. 119205 showed a significantly higher CDocker score of 30.8343 and a more favorable binding energy of −145.23 kcal/mol, suggesting a strong binding affinity. In addition, the LUDI analysis revealed significant interactions between 119205 and key residues in the ALR2 binding pocket. These interactions involve hydrogen bonds with Leu301, Gln183, and Lys77, as well as pi-pi stacking interactions with Phe122, Tyr209, and Tyr48. These particular molecular interactions indicate that 119205 binding interactions within the ALR2 binding pocket are robust and targeted. The C. melo compound CID 119205 has a balanced pharmacophore model that combines hydrophobic interactions, pi-pi stacking, and hydrogen bonds, as demonstrated by the docking and simulation results. Together, these characteristics improve its binding affinity and ability to inhibit ALR2. The significance of these interactions was further supported by the LUDI analysis, which also revealed that CID 119205 has a higher CDocker score and a more favorable binding energy than the reference inhibitor Epalrestat, Fig. 1 and Table 4.

3.3. Molecular dynamics exploration of PubChem CID: 110205 in complex with ALR2Protein and ligand RMSD

The control complex exhibits relatively low average RMSD values in protein and ligand, indicating overall stability and minimal

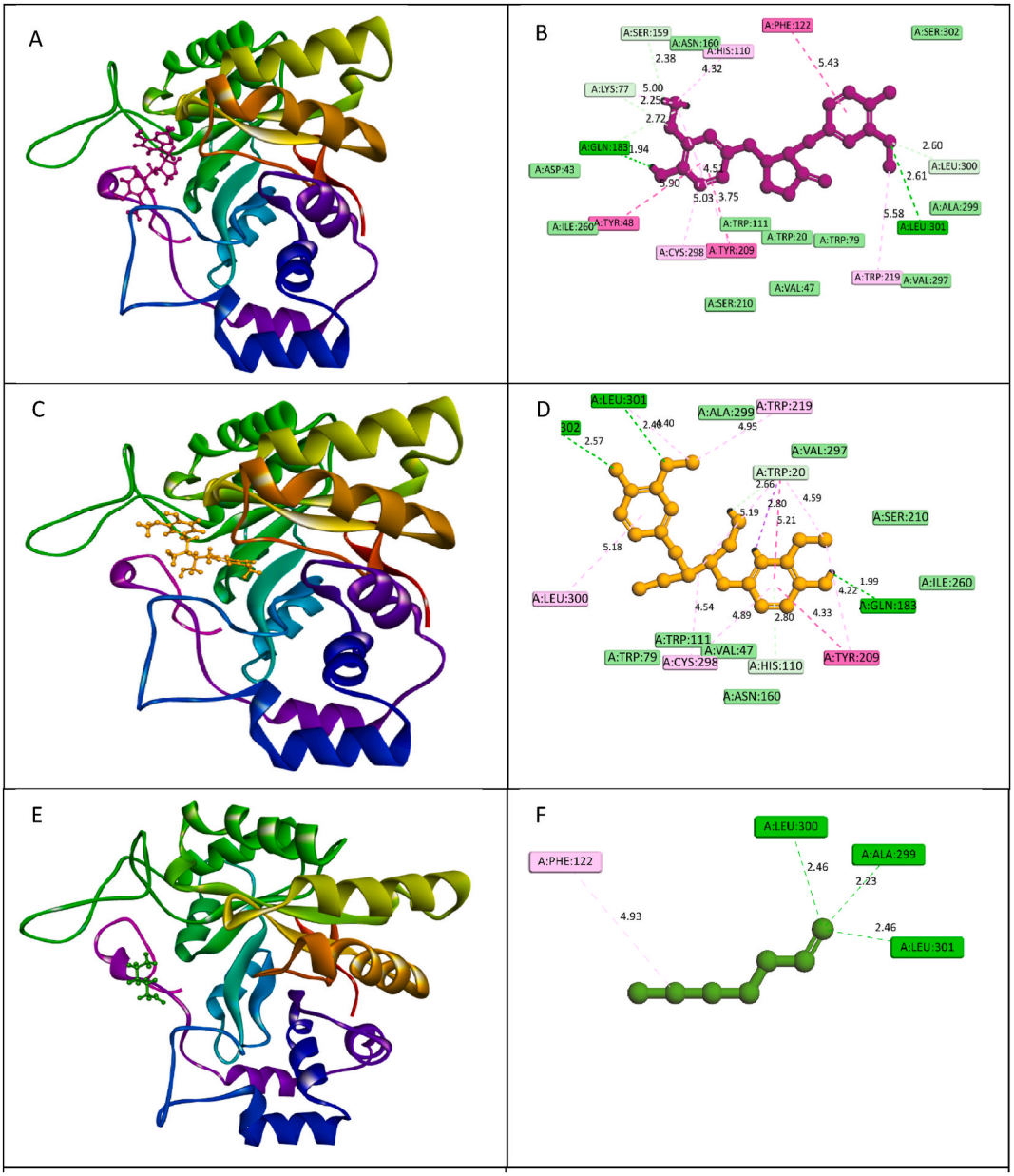

Fig. 1. Molecular docking results of *C. melo* compounds with ALR2 protein. The 3D and 2D images illustrate the critical interactions formed between the compounds and specific protein residues. Key residues involved are highlighted, and the distances between the compound and residues are annotated in angstroms on the dashed lines, where Figures A and B (Compound: 119205), Figures C and D (Compound: 65373), Figures E and F (Compound: 6184), Figures G and H (Compound: 332427), and Fig. I and J (Compound: Epalrestat) are showing 3D and 2D interactions, respectively.

deviation from the initial structure. While in the docked complex the protein RMSD is slightly lower than in the control complex, the ligand RMSD is higher and shows increasing fluctuations over time, suggesting greater conformational changes and mobility of the ligand within the binding pocket, as shown in Fig. 2.

3.4. Protein RMSF (root mean square fluctuations)

Both cases show similar average protein RMSF values, indicating comparable flexibility and dynamics of the protein residues during the simulation, Fig. 3. Both cases exhibit similar average protein radius of gyration values, suggesting similar compactness or overall shape of the protein structure throughout the simulation.

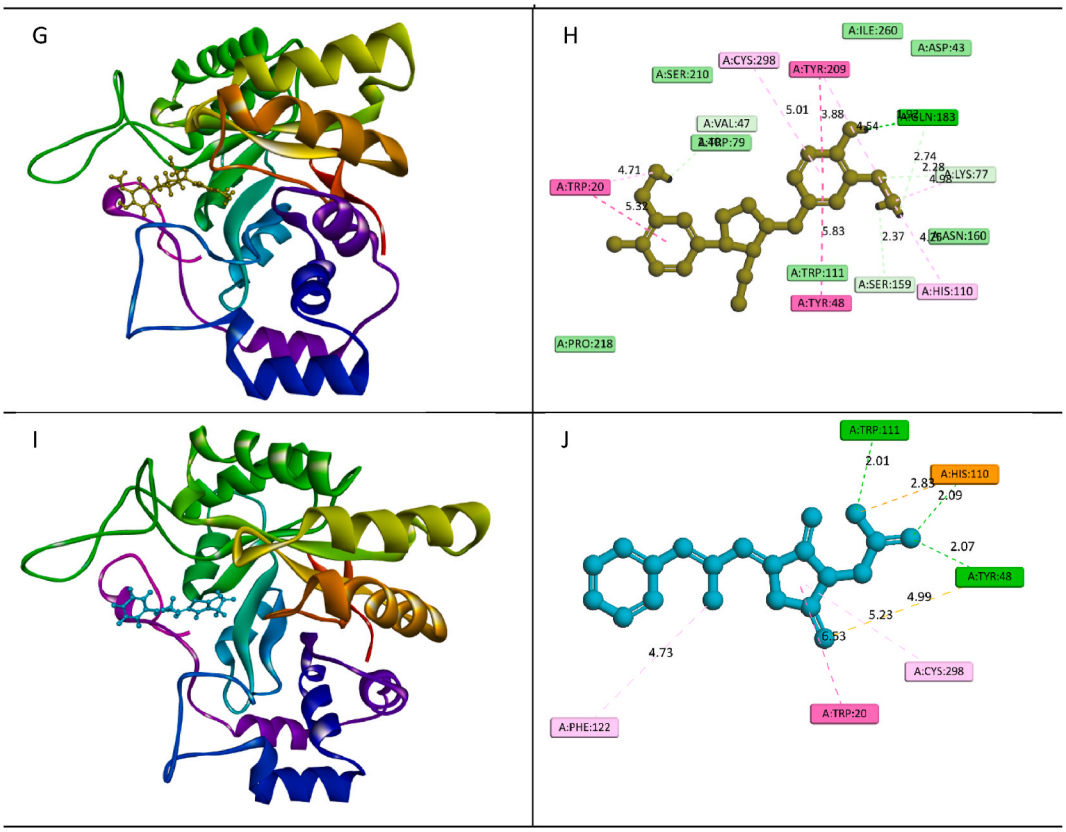

Fig. 1. (*continued*).

3.5. Hydrogen bonds between ligand-protein

The control complex shows a higher average number of hydrogen bonds between the ligand and protein as compared to the docked complexes, however, the docked complex exhibits fewer hydrogen bonds, Fig. 4.

3.6. Center of mass distance between ligand-protein

The control complex shows a higher average center of mass distance between the ligand and protein compared to the docked complex, indicating a greater separation between the two molecules. The ligand leaves the binding pocket in the first 20 ns and then rebinds with the protein after 20 ns till 100 ns. Conversely, the docked complex exhibits a lower average distance, suggesting closer proximity and potentially stronger binding between the ligand and protein. The ligand remained in bound form throughout the simulation time, Fig. 5.

3.7. Binding pocket dynamics

In the Control complex, the ligand leaves the binding pocket within the first 20 ns of simulation but it later rebinds with fluctuations, indicating dynamic binding and potential ligand dissociation and re-association events. In contrast, the docked ligand remains intact within the binding pocket throughout the 100 ns of simulation, suggesting stable and persistent binding, Fig. 6.

4. MMGBSA binding energy

The docked ligand exhibits a significantly lower average MMGBSA binding energy compared to the Control ligand, indicating stronger and more favorable binding between the ligand and protein in the docked complex, Fig. 7. Overall, the comparison highlights differences in the stability, dynamics, and binding properties of the control complexes in control and docked systems. These differences may arise from variations in the molecular structure of the ligand, protein conformational changes, or environmental conditions during the simulations.

Polyphenols have a wide range of modes in which they interact with target receptor proteins. These include directly binding to protein targets, influencing enzyme activity, controlling gene expression, and providing antioxidant and anti-inflammatory effects.

Table 4
Intramolecular interactions and scores of the *C. melo compounds* and ALR2.

Name	-CDOCKER Score	Binding Energy (Kcal/mol)	Ligand Efficiency Score LEHA	LUDI 3	Interacting Residues
119205	30.8343	−145.23	81.2	1021	Hydrogen Bond: Leu301, Gln183, Lys77, Leu300, Ser159, Gln183. Pi-Pi Stacking: Phe122, Tyr209, Tyr48. Alkyl: Lys77. Pi-Alkyl: His110, Tyr209, Trp219, Cys298.
65373	25.3692	−120.23	78.1	890	Hydrogen Bond: Leu301, Ser302, Gln183, His110, Trp20. Pi-Sigma: Trp20. Pi-Pi Stacking: Tyr209, Trp20. Alkyl: Cys298, Leu301. Pi-Alkyl: Cys298, Leu301, Trp20, Tyr209, Trp219, Cys298, Leu300.
6184	18.67	−38.58	69.73	264	Hydrogen Bond: Ala299, Leu300, Leu301. Pi Alkyl Bond: Phe122.
332427	15.3902	−60.3	58.76	832	Hydrogen Bond: Gln183, Lys77, Val47, Ser159. Pi-Pi Stacking: Tyr209. Pi-Pi T-shaped: trp20, Tyr48. Alkyl: Lys77. Pi-Alkyl: Trp20, His110, Tyr209, Cys298.
Epalrestat	14.17	−148.18	33.56	732	Hydrogen Bond: Tyr48, His110, Trp111. Electrostatic: His110. Pi-sulfur: Tyr48. Pi-Pi stacking: Trp20. Pi Alkyl: Phe122, cys298.
702	10.37	−15.44	76.4	193	Hydrogen Bond: Ala299, Leu300, Cys298. Alkyl Bond: Ala299, Ley301. Pi Alkyl Bond: Trp219.
73399	5.02137	−30.45	69.35	1006	Hydrogen Bond: trp111, Asn160, Ser302, Gln183, His110, Tyr209. Pi-Sulfur: Cys298. Pi-Pi T-shaped: Trp20. Alkyl: Lys77. Pi-Alkyl: His110, Tyr209.
5362720	4.20	−42.92	54.39	340	Hydrogen Bond: Ala299, Leu300, Leu301. Alkyl Bond: Pro218. Pi Alkyl Bond: Trp219.

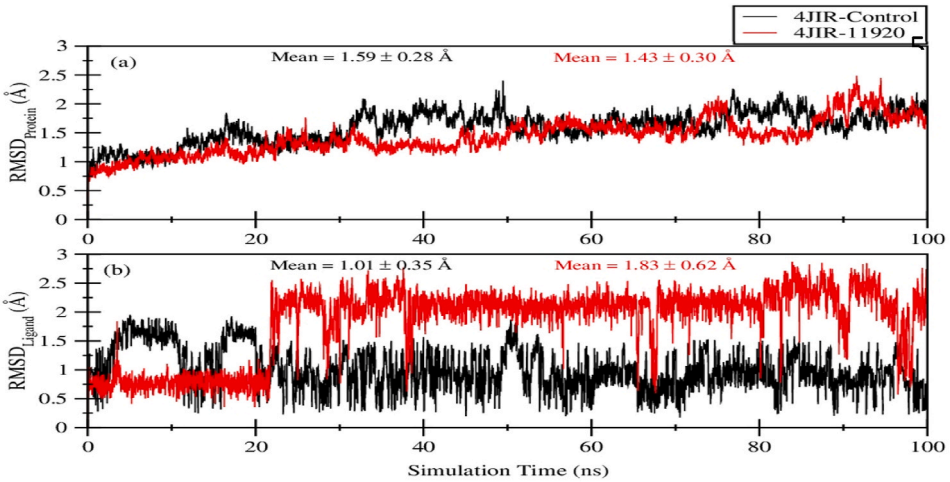

Fig. 2. The Ca-RMSD calculated for the 4JIR protein (a) complexed with 01_Control (Black line), and (b) 02_Docked (red line) using the Bio3D module of R. The mean and standard deviations are also calculated. (b) RMSD for ligands.

Polyphenols are highly promising as therapeutic candidates for a range of diseases and conditions due to their structural diversity and capacity to interact with multiple cellular targets [50]. The compound, CID: 119205, also known as (−)-Matairesinol, has a complex structure and is classified as a polyphenolic compound. The structure of this compound includes multiple benzene rings. These aromatic rings are essential for its interaction with receptor proteins, especially through pi-pi stacking interactions. The compound is

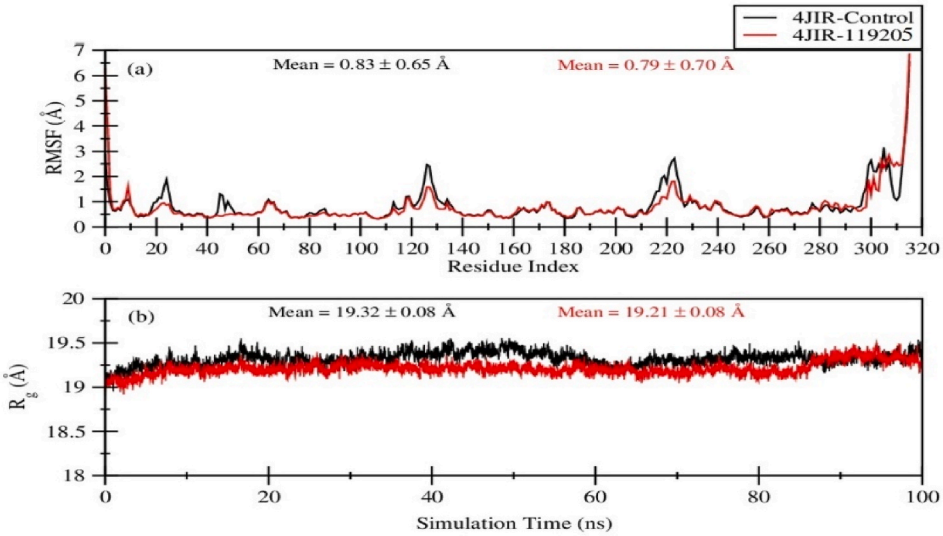

Fig. 3. (a) The Ca-RMSF calculated for the 4JIR protein complexed with 01_Control (black line), and 02_Docked (red line) using Bio3D module of R. (b) The Ca-RoG calculated for the 4JIR protein complexed with 01_Control (black line), and 02_Docked (red line) using the Bio3D module of R.

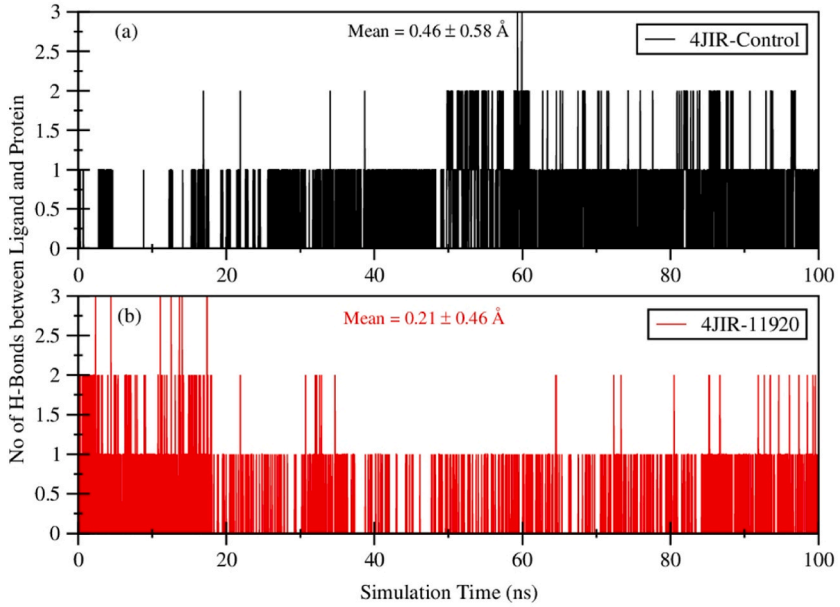

Fig. 4. The number of hydrogen bonds formed between the binding site of 4JIR protein and (a) 01_Control, and (b) 02_Docked during a simulation time of 100 ns.

composed of ether linkages (-O-) that connect different aromatic rings and aliphatic chains. These ether linkages can engage in hydrogen bonding interactions with polar residues found in the binding pocket of receptor proteins, thereby increasing the compound's binding affinity. The presence of an aliphatic chain in (−)-Matairesinol imparts flexibility to the molecule. The compound can take on various conformations, which helps it interact effectively with the receptor protein by adjusting to the shape and size of the binding pocket. Through pi-pi stacking interactions, the aromatic rings in (−)-matairesinol can effectively bind to aromatic residues in the receptor protein's binding pocket. These interactions play a crucial role in enhancing the compound's binding affinity by expanding the contact surface and facilitating favorable van der Waals interactions [51].

5. Conclusion

This study examines the particular inhibition of ALR2. Considering that this enzyme is the primary target protein in diabetes. This

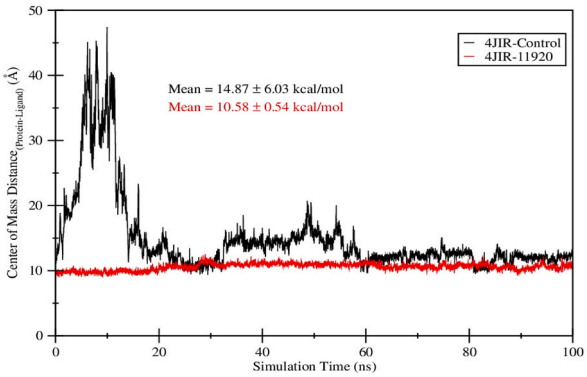

Fig. 5. The distance fluctuation between the center-of-mass (CoM) of 4JIR protein and the center-of-mass of 01_Control (black line), and 02_Docked (red line) ligands during simulation time of 100ns. The CoM distance was evaluated using the gmx_distance command. The mean and standard deviations are also calculated. In 01_control, the ligand left the binding site for first 20 ns and after 20 ns it remained intact with the same binding site as it was earlier in initial position. The 02_docked ligands remained bound throughout the simulation time.

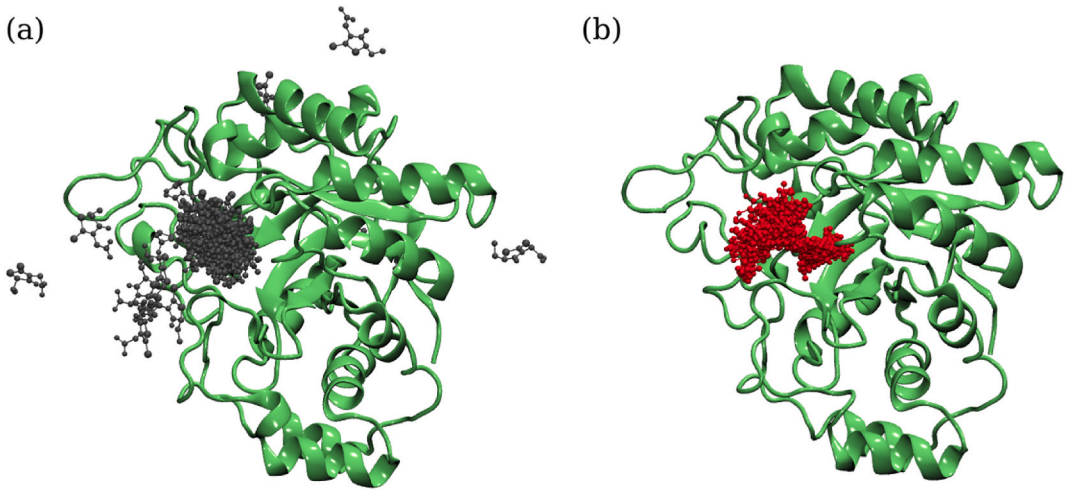

Fig. 6. Snapshots of 01_Control (a), and 02_Docked (b) complexes taken after every 1 ns of MD simulation (total 100 snapshots of ligands). In this snapshot, the protein is fixed at 0 ns. This indicates that 01_Control ligands briefly left the protein while 02_Docked ligands remained in a bound state during simulation time. This is also supported by the distance fluctuation between the center-of-mass (CoM) of 4JIR protein and the center-of-mass of 01_Control (black line).

investigation aimed to identify potential therapeutic inhibitors with pharmacological relevance in *C. melo.* Molecular docking, ligand scoring, and MD simulation were utilized to determine potential inhibitors for the ALR2 and to investigate the organization of interaction, as well as the contribution of particular regions and residues to the binding of inhibitors to the active site of the protein. These inhibitors compete with the inhibitor binding site to restrict ALR2 activity. The MD simulation revealed that PubChem CID 119205, a compound with a robust interaction, remained stable with the smallest deviation from the interaction site over the course of the entire observed simulation duration. The findings revealed that it exhibits stronger binding to epalrestat. Hence, it may be a suitable alternative for diabetes treatment. Further investigation is required to validate the inhibitory activity of PubChem CID 119205 against ALR2 and to evaluate its safety, efficacy, and pharmacokinetic profiles in diabetic models. In future studies, we plan to conduct comprehensive off-target interaction analyses, encompassing comparative docking studies with related enzymes and proteins, as well as experimental validation through enzyme inhibition assays and cell-based studies. Such studies would ultimately contribute to the development of this compound as a potential anti-diabetic therapeutic.

Consent for publication

Not applicable.

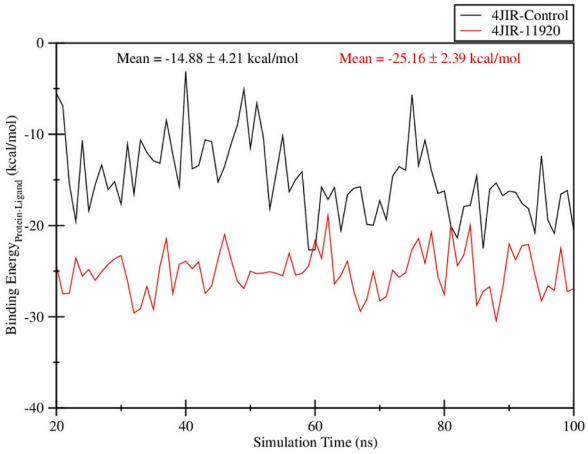

Fig. 7. The Molecular mechanics Generalize-Born surface area (MMGBSA) Gibb's free binding energies calculated after every 1ns snapshot of 4JIR protein complexed with 01_Control (black line), and 02_Docked (red line) ligands. The mean and standard deviations are calculated for the last 80 ns of the trajectory after excluding the first 20 ns. The 02_Docked ligand binds better with the protein as compared with the 01_Control.

Funding

This research has been funded by Scientific Research Deanship at University of Ha'il - Saudi Arabia through project number RG-21 162.

CRediT authorship contribution statement

Khalid Alshaghdali: Visualization, Investigation, Funding acquisition, Conceptualization. **Munazzah Tasleem:** Writing – review & editing, Writing – original draft, Methodology. **Raja Rezgui:** Writing – original draft, Validation, Investigation. **Talal Alharazi:** Visualization, Software, Project administration, Formal analysis. **Tolgahan Acar:** Validation, Supervision, Software, Methodology. **Raed Fahad Aljerwan:** Writing – review & editing, Writing – original draft, Software. **Ahmed Altayyar:** Investigation, Formal analysis. **Samra Siddiqui:** Writing – review & editing, Supervision. **Mohd Saeed:** Writing – review & editing, Writing – original draft, Methodology, Conceptualization. **Dharmendra Kumar Yadav:** Writing – review & editing, Writing – original draft, Methodology. **Amir Saeed:** Writing – review & editing, Project administration, Conceptualization.

Declaration of competing interest

The authors declare that they have no known competing financial interests or personal relationships that could have appeared to influence the work reported in this paper.

Acknowledgements

This research has been funded by Scientific Research Deanship at University of Ha'il - Saudi Arabia through project number RG-21 162.

Appendix A. Supplementary data

Supplementary data to this article can be found online at https://doi.org/10.1016/j.heliyon.2024.e35255.

References

[1] D.P. Schuster, V. Duvuuri, Diabetes mellitus, Clin. Podiatr. Med. Surg. 19 (1) (2002) 79–107.
[2] L. Wang, et al., Trends in prevalence of diabetes and control of risk factors in diabetes among US adults, 1999-2018, JAMA 326 (8) (2021) 1–13.
[3] Y. Zheng, S.H. Ley, F.B. Hu, Global aetiology and epidemiology of type 2 diabetes mellitus and its complications, Nat. Rev. Endocrinol. 14 (2) (2018) 88–98.
[4] M. Zhou, et al., Mortality, morbidity, and risk factors in China and its provinces, 1990-2017: a systematic analysis for the Global Burden of Disease Study 2017, Lancet 394 (10204) (2019) 1145–1158.
[5] A. Fatima, et al., Type 1 and type 2 diabetes mellitus: are they mutually exclusive? Singap. Med. J. 54 (7) (2013) 396–400.
[6] R. Nagarathna, et al., Prevalence of diabetes and its determinants in the young adults Indian population-call for yoga intervention, Front. Endocrinol. 11 (2020).

[7] M.M.V. Rao, T.P.N. Hariprasad, In silico analysis of a potential antidiabetic phytochemical erythrin against therapeutic targets of diabetes, In Silico Pharmacol 9 (1) (2021) 5.
[8] D. Selvarajah, et al., Diabetic peripheral neuropathy: advances in diagnosis and strategies for screening and early intervention, Lancet Diabetes Endocrinol. 7 (12) (2019) 938–948.
[9] J. Zhu, et al., Diabetic peripheral neuropathy: pathogenetic mechanisms and treatment, Front. Endocrinol. 14 (2023) 1265372.
[10] A.G. Atanasov, et al., Natural products in drug discovery: advances and opportunities, Nat. Rev. Drug Discov. 20 (3) (2021) 200–216.
[11] T.V. Fiorentino, et al., Hyperglycemia-induced oxidative stress and its role in diabetes mellitus related cardiovascular diseases, Curr. Pharmaceut. Des. 19 (32) (2013) 5695–5703.
[12] M. Kumar, et al., Addressing selectivity issues of aldose reductase 2 inhibitors for the management of diabetic complications, Future Med. Chem. 12 (14) (2020) 1327–1358.
[13] M. Saeed, et al., Identification of putative plant-based ALR-2 inhibitors to treat diabetic peripheral neuropathy, Curr. Issues Mol. Biol. 44 (7) (2022) 2825–2841.
[14] A. Imran, et al., Development, molecular docking, and in silico ADME evaluation of selective ALR2 inhibitors for the treatment of diabetic complications via suppression of the polyol pathway, ACS Omega 7 (30) (2022) 26425–26436.
[15] M. Saeed, et al., Assessment of antidiabetic activity of the shikonin by allosteric inhibition of protein-tyrosine phosphatase 1B (PTP1B) using state of art: an in silico and in vitro tactics, Molecules 26 (13) (2021).
[16] P. Zhang, et al., Oxidative stress and diabetes: antioxidative strategies, Front. Med. 14 (5) (2020) 583–600.
[17] C. Ononamadu, A. Ibrahim, Molecular docking and prediction of ADME/drug-likeness properties of potentially active antidiabetic compounds isolated from aqueous-methanol extracts of Gymnema sylvestre and Combretum micranthum, Biotechnologia 102 (1) (2021) 85–99.
[18] P. Sebastian, et al., Cucumber (Cucumis sativus) and melon (C. melo) have numerous wild relatives in Asia and Australia, and the sister species of melon is from Australia, Proc. Natl. Acad. Sci. USA 107 (32) (2010) 14269–14273.
[19] A. Pandey, et al., Studies on fruit morphology, nutritional and floral diversity in less-known melons (Cucumis melo L.) of India, Genet. Resour. Crop Evol. 68 (4) (2021) 1453–1470.
[20] V.K. Vishwakarma, J.K. Gupta, P.K. Upadhyay, Pharmacological importance of Cucumis melo L.: an overview, Asian J. Pharmaceut. Clin. Res. (2017) 8–12.
[21] A.K. Srivastava, A. Mukerjee, A. Tripathi, Antidiabetic and antihyperlipidemic activities of Cucumis melo var. momordica fruit extract on experimental animals, Future Journal of Pharmaceutical Sciences 6 (1) (2020) 92.
[22] N. Tran, B. Pham, L. Le, Bioactive compounds in anti-diabetic plants: from herbal medicine to modern drug discovery, Biology 9 (9) (2020).
[23] Y. Wang, et al., PubChem: a public information system for analyzing bioactivities of small molecules, Nucleic Acids Res. 37 (suppl_2) (2009) W623–W633.
[24] K. Mohanraj, et al., IMPPAT: a curated database of Indian medicinal plants, Phytochemistry and therapeutics, Sci. Rep. 8 (1) (2018) 4329.
[25] L. Zhang, et al., Inhibitor selectivity between aldo-keto reductase superfamily members AKR1B10 and AKR1B1: role of Trp112 (Trp111), FEBS Lett. 587 (22) (2013) 3681–3686.
[26] A.L. Hopkins, et al., The role of ligand efficiency metrics in drug discovery, Nat. Rev. Drug Discov. 13 (2) (2014) 105–121.
[27] L. Jena, U. Nayak, Theories of Career Development: an Analysis, 2020.
[28] M. Tasleem, et al., Investigation of antidepressant properties of yohimbine by employing structure-based computational assessments, Curr. Issues Mol. Biol. 43 (3) (2021) 1805–1827.
[29] A.d. Alwan, Noncommunicable Diseases: a Major Challenge to Public Health in the Region, 1997.
[30] H. Mohamed, et al., Knowledge, attitude, and practice of type2 Arab diabetic patients in Qatar: a cross-sectional study, Int. J. Diabetes Dev. Ctries. 35 (2) (2015) 205–209.
[31] S. Wang, et al., Docking-based virtual screening of TβR1 inhibitors: evaluation of pose prediction and scoring functions, BMC Chemistry 14 (1) (2020) 52.
[32] H.-J. Böhm, LUDI: rule-based automatic design of new substituents for enzyme inhibitor leads, J. Comput. Aided Mol. Des. 6 (1992) 593–606.
[33] R.C. Mohs, N.H. Greig, Drug discovery and development: role of basic biological research, Alzheimers Dement (N Y) 3 (4) (2017) 651–657.
[34] P.W. Kenny, The nature of ligand efficiency, J. Cheminf. 11 (1) (2019) 8.
[35] J. Lee, et al., CHARMM-GUI input generator for NAMD, GROMACS, AMBER, OpenMM, and CHARMM/OpenMM simulations using the CHARMM36 additive force field, Biophys. J. 110 (3) (2016) 641a.
[36] S. Jo, et al., *CHARMM-GUI*: a web-based graphical user interface for CHARMM, J. Comput. Chem. 29 (11) (2008) 1859–1865.
[37] K.A. Qureshi, et al., In vitro and in silico approaches for the antileishmanial activity evaluations of actinomycins isolated from novel Streptomyces smyrnaeus strain UKAQ_23, Antibiotics 10 (8) (2021) 887.
[38] M.J. Abraham, et al., GROMACS: high performance molecular simulations through multi-level parallelism from laptops to supercomputers, SoftwareX 1 (2015) 19–25.
[39] J. Huang, et al., CHARMM36m: an improved force field for folded and intrinsically disordered proteins, Nat. Methods 14 (1) (2017) 71–73.
[40] I.I.I.B.R. Miller, et al., MMPBSA. py: an efficient program for end-state free energy calculations, J. Chem. Theor. Comput. 8 (9) (2012) 3314–3321.
[41] B.K. Rajendran, et al., Pharmacoinformatic approach to explore the antidote potential of phytochemicals on bungarotoxin from Indian Krait, Bungarus caeruleus, Comput. Struct. Biotechnol. J. 16 (2018) 450–461.
[42] Q. Pu, et al., Designing and screening of fluoroquinolone substitutes using combined in silico approaches: biological metabolism–bioconcentration bilateral selection and their mechanism analyses, Green Chem. 24 (9) (2022) 3778–3793.
[43] S. Tesfaye, G. Sloan, Diabetic polyneuropathy - advances in diagnosis and intervention strategies, Eur. Endocrinol. 16 (1) (2020) 15–20.
[44] B.K. Rajendran, et al., Pharmacoinformatic approach to explore the antidote potential of phytochemicals on bungarotoxin from Indian krait, Bungarus caeruleus, Comput. Struct. Biotechnol. J. 16 (2018) 450–461.
[45] S. Fatima, et al., ADMET profiling of geographically diverse phytochemical using chemoinformatic tools, Future Med. Chem. 12 (1) (2020) 69–87.
[46] M. Berry, B. Fielding, J. Gamieldien, Chapter 27 - practical considerations in virtual screening and molecular docking, in: Q.N. Tran, H. Arabnia (Eds.), Emerging Trends in Computational Biology, Bioinformatics, and Systems Biology, Morgan Kaufmann, Boston, 2015, pp. 487–502.
[47] J. Ainsley, et al., Chapter one - combined quantum mechanics and molecular mechanics studies of enzymatic reaction mechanisms, in: T.G. Karabencheva-Christova, C.Z. Christov (Eds.), Advances in Protein Chemistry and Structural Biology, Academic Press, 2018, pp. 1–32.
[48] F. Stanzione, I. Giangreco, J.C. Cole, Chapter Four - use of molecular docking computational tools in drug discovery, in: D.R. Witty, B. Cox (Eds.), Progress in Medicinal Chemistry, Elsevier, 2021, pp. 273–343.
[49] R.T. Kroemer, Structure-based drug design: docking and scoring, Curr. Protein Pept. Sci. 8 (4) (2007) 312–328.
[50] N. Yahfoufi, et al., The immunomodulatory and anti-inflammatory role of polyphenols, Nutrients 10 (11) (2018).
[51] I.F. do Valle, et al., Network medicine framework shows that proximity of polyphenol targets and disease proteins predicts therapeutic effects of polyphenols, Nature Food 2 (3) (2021) 143–155.